Nanoscale

PAPER

View Article Online
View Journal | View Issue

Cite this: *Nanoscale*, 2017, **9**, 12051

Time-resolved nanomechanics of a single cell under the depolymerization of the cytoskeleton†

Pablo D. Garcia,‡ Carlos R. Guerrero‡ and Ricardo Garcia *

Received 14th May 2017,
Accepted 20th July 2017

DOI: 10.1039/c7nr03419a

rsc.li/nanoscale

Single cell stiffness measurements consider cells as passive and elastic materials which react instantaneously to an external force. This approximation is at odds with the complex structure of the cell which includes solid and liquid components. Here we develop a force microscopy method to measure the time and frequency dependencies of the elastic modulus, the viscosity coefficient, the loss modulus and the relaxation time of a single live cell. These parameters have different time and frequency dependencies. At low modulation frequencies (0.2–4 Hz), the elastic modulus remains unchanged; the loss modulus increases while the viscosity and the relaxation time decrease. We have followed the evolution of a fibroblast cell subjected to the depolymerization of its F-actin cytoskeleton. The elastic modulus, the loss modulus and the viscous coefficient decrease with the exposure time to the depolymerization drug while the relaxation time increases. The latter effect reflects that the changes in the elastic response happen at a higher rate than those affecting the viscous flow. The observed behavior is compatible with a cell mechanical response described by the poroelastic model.

1. Introduction

Eukaryotic cells modify their shape and mechanical response in the presence of either intrinsic or extrinsic cues of forces. Atomic Force Microscopy (AFM) is being widely used to measure the mechanical response of single cells.[1–11] Most AFM experiments measure the elastic response (stiffness) of the cytoplasm, the cortex and the nucleus. In some cases, the AFM data have revealed remarkable changes in the elastic response of cells under different physiological conditions. In particular, stiffness indicators are applied to track different physiological and pathological processes in cells[12–22] or the surrounding extra cellular matrix.[23,24]

The cytoplasm consists of solid elements such as cytoskeleton, organelles and ribosomes in a liquid fluid (cytosol).[25,26] Several experiments have demonstrated the existence of viscous processes in the cytoskeleton remodeling and in the inner cell dynamics.[26–28] In fact, stiffness measurements performed on cancer cells of different pathological degrees[17,29,30] have given similar elastic (Young) moduli values. These findings could be related to the limitations of stiffness measurements to describe the mechanical state of a cell.

Several factors explain the extensive use of AFM stiffness studies on cells. (1) The existence of an established protocol to determine the elastic modulus from force–distance curves.[31,32] (2) Stiffness measurements have provided insightful information about the mechanics and physiology of cells.[1,3] (3) On the other hand, there is not an established AFM protocol to perform time or frequency-dependent experiments.[33–38] In addition, there are several competing theoretical models to interpret the data.[40–43]

Let's summarize the AFM studies devoted to measure the viscoelastic properties of cells. These contributions can be broadly classified into two main categories, force oscillation and time response methods. In a force oscillation experiment, the tip is indented on the cell to a given depth and a subsequent sinusoidal perturbation is applied.[28,33,38] Multi-harmonic AFM experiments[8,36,39] could also be included in this category although in multi-harmonic experiments there is not a distinction between the indentation and the oscillation stages. Force oscillation approaches require the use of an elaborated theoretical framework.[36] In many cases, it is not always possible to deduce parameters that could be compared with the elastic modulus and viscous coefficient obtained from force–distance curves. As an alternative, the loss tangent of a cell has been measured.[29,36] This parameter represents the ratio between the energy dissipated and the energy stored in one cycle of the oscillation.[44] The loss tangent avoids the estimation of the tip radius. However, this parameter has not been a straightforward link to the mechanical properties of a cell.

Materials Science Factory, Instituto de Ciencia de Materiales de Madrid, CSIC, c/ Sor Juana Ines de la Cruz 3, 28049 Madrid, Spain. E-mail: r.garcia@csic.es

†Electronic supplementary information (ESI) available. See DOI: 10.1039/c7nr03419a

‡These authors contributed equally to this work.

Time response methods include two different approaches, load relaxation and creep compliance experiments. In a load relaxation experiment,[26,35,45] the tip is moved towards the cell until a certain indentation is reached, then the tip is held still and the dependence of the force with time is recorded. Creep compliance experiments[33,34,37] keep the force applied on the cell at a fixed value. Due to the cell internal reorganization processes, keeping a constant force requires a continuous change in the z-position of the cell support. Time response methods require theoretical models to transform the data into rheological parameters. These models have to deal with the determination of the contact area for a viscoelastic contact. In general, time response methods are not compatible with high resolution imaging.

Force microscopy offers other schemes to measure inelastic interactions. The force–distance curves obtained during an approach–retraction cycle usually show the presence of a hysteresis loop. The area enclosed by the loop determines the energy dissipated by the tip–sample interaction[46–48] (energy hysteresis). The measurement of the energy hysteresis could provide a method to determine the viscoelastic properties within the cell.[49] The transformation of energy hysteresis values into nanomechanical properties implies two stages. First, it requires the existence of well-defined models in the energy dissipation processes.[50] Second, these models require the determination of the contact area during the approach–retraction cycle. Currently, there are no analytical expressions to determine the contact area in the presence of viscoelastic processes.

Here we develop a force microscopy method to determine the time and frequency responses of a single live cell under the influence of an external compressive force. The method determines the Young's (elastic) modulus, the loss modulus, the viscosity coefficient and the relaxation time of a cell as a function of the frequency of the external force. This method can be divided in two main steps, the acquisition of force–distance curves and the application of a model to extract the cell rheological response from these curves. The elastic and dissipative components of the force are determined by considering the approach and retraction sections of the force–distance curve around the maximum indentation. Finite element simulation shows that near the maximum indentation the contact area is well described by conventional contact mechanics models. The method has been applied to follow the evolution of a single fibroblast cell exposed to the action of an actin polymerization inhibitor drug. The elastic modulus, the viscous coefficient and the loss modulus decrease while the relaxation time increases with the exposure time to the drug.

2. Theoretical model

The tensorial stress–strain relationship for a linear viscoelastic material can be expressed using the relaxation function[51,52] $\Psi(t)$. This function is deduced from one-dimensional approximations[49] that describe the stress response to a unit change of strain in the system. These approximations do not consider the change of the contact area with the indentation nor the tip geometry. However, these factors should be taken into account to reach a satisfactory numerical interpretation of the AFM data.

A realistic description of a three-dimensional system should consider that the vertical and lateral deformations are coupled. For this system, the dependence of the force with the deformation in the presence of viscoelastic processes is obtained by combining the relaxation function $\Psi(t)$ with the known force–indentation relationship obtained for an elastic material of the same geometry.[53] This step involves the replacement of the elastic (Young) modulus E in the elastic equation for an integral operator that is expressed in terms of the relaxation function $\Psi(t)$. The process for a three-dimensional axisymmetric indenter starts with the expression that relates the force with the indentation for an elastic material

$$F = \alpha E I^{\beta} \tag{1}$$

where $I(t)$ is the indentation, α is a coefficient that depends on the geometry and the Poisson coefficient and β is a geometric factor. These coefficients depend on the contact mechanics model. If we substitute E by the relaxation function $\Psi(t)$, we obtain the force exerted on a cell (viscoelastic material) as a function of time that can be expressed as

$$F(t) = \alpha \int_0^t \psi(t - t') \frac{\mathrm{d}}{\mathrm{d}t'} [I(t')^{\beta}] \mathrm{d}t' \tag{2}$$

To express $\Psi(t)$ in terms of mechanical properties requires the use of a viscoelastic model. This step needs to balance numerical accuracy and the capability to provide an analytical expression in a closed form. The standard linear solid model provides an accurate approach to determine creep and relaxation processes.[52] However, this model does not allow deducing expressions in a closed form when the contact area depends on the indentation. The above dependence should always be considered because the force–distance curves on cells involve indentations of several micrometers.

On the other hand, the Kelvin–Voigt model[52] enables deducing analytical expressions to link the parameters with the observables without restricting the variation of the contact area with the deformation. For a given frequency, we demonstrate that the results provided by the Kelvin–Voigt model are equivalent to those given by any other linear viscoelastic model, in particular, the standard linear solid model (see the ESI†). Then,

$$\psi(t) = E + \eta_{\mathrm{com}} \delta(t) \tag{3}$$

where $\delta(t)$ is the Dirac delta function and η_{com} is the compressive viscoelastic coefficient (also known as the Trouton coefficient). Force–distance measurements involve the application of compressive forces normal to the cell surface. We remark that inside the cell the force is released in normal and lateral directions.

In many contributions the viscosity is described in terms of the one-dimensional laminar flow model. In this model the relevant coefficient is the shear viscous coefficient η_{sh}. For an incompressible material (ν = 0.5), the compressive and shear viscous coefficients are related by

$$\eta_{com} = 3\eta_{sh} \quad (4)$$

In the following we express our results in terms of the commonly used shear viscous coefficient $\eta_{sh} = \eta$. With the above assumptions the force is calculated using the following equation:

$$F(t) = \alpha I(t)^{\beta-1}[3\beta\eta\dot{I}(t) + EI(t)] \quad (5)$$

The above expression can be simplified for Hertz and Sneddon contact mechanics models. For the latter (conical geometry),

$$\alpha = \frac{1}{1-\nu^2}\frac{2\tan(\phi)}{\pi} \quad (6)$$

β = 2, ν is the Poisson coefficient and ϕ is the cone semi-angle.

The interaction force includes conservative (elastic) F_c and dissipative (inelastic) F_{dis} processes. In general the force can be expressed as

$$F(t) = F_c + F_{dis} \quad (7)$$

where

$$F_c(t) = \frac{8}{3}\frac{\tan(\phi)}{\pi}EI^2(t) \quad (8)$$

$$F_{dis}(t) = 16\frac{\tan(\phi)}{\pi}\eta I(t)\frac{dI(t)}{dt} \quad (9)$$

In eqn (9) the force is proportional to the indentation. This result is different from a previous expression deduced without the above considerations.[50]

The loss modulus is calculated from the expression (see the ESI†)

$$E_{loss} = -i\omega\eta \quad (10)$$

In the following only absolute values of E_{loss} are reported.

To deduce an expression for the relaxation time, we assume the Kelvin–Voigt approximation, where an initial deformation I_0 decays exponentially with time,

$$I(t) = I_0 e^{-\frac{t}{\tau}} \quad (11)$$

where the relaxation time is defined by

$$\tau = \frac{\eta}{E} \quad (12)$$

3. Materials and methods

3.1 Force microscopy and force spectroscopy

All the AFM experiments were performed in a cell culture medium with HEPES (10 mM) (see below) using a commercial instrument (JPK NanoWizard 3, JPK Instruments AG, Berlin, Germany) mounted on an Axio Vert. A1 inverted microscope (Carl Zeiss, Oberkochen, Germany). To ensure that the cells stay alive and adherent during the force spectroscopy experiments, the measurements were performed at a constant temperature of 37 °C. We have used MLCT-B cantilevers (Bruker, Camarillo, CA, USA) with a nominal spring constant of 0.02 N m^{-1} and a conical tip shape with a nominal half opening angle of 18°. In order to obtain reliable and quantitative data from the AFM experiments, the cantilever spring constant k was calibrated using the thermal tuning method. The maximum force applied to the cells was 3.0 nN.

The hydrodynamic drag due to the interaction of the cantilever body with the liquid causes an additional hysteresis in the force curve.[55,56] The hysteresis is characterized by the separation between the baselines of the approach and withdrawing sections of a force curve. We have developed an algorithm to correct the data from the drag effect (see the ESI†).

Force–distance curves. The tip–sample distance has been modulated by applying a triangular waveform. The data acquisition rate has been calculated to be 4000 Hz. Bottom effect corrections for a conical tip have been applied to correct the cell finite thickness.[7] The force–distance curves have been measured on a region above the nucleus.

3.2 Cell culture and sample preparation

Mouse Embryonic Fibroblasts (MEFs) were cultured at 37 °C in Dulbecco's Modified Eagle Medium – DMEM (Gibco Life Technologies, Paisley, UK) supplemented with 10% Fetal Bovine Serum – FBS (Gibco Life Technologies) and 1% penicillin/streptomycin at controlled humidity (90%) and CO_2 concentration (5%). A 60 mm Petri dish (Thermo Fisher Scientific, Massachusetts, USA) contains the cells during the cell culture process. Upon removal from the incubator, a 10 mM HEPES (4-(2-hydroxyethyl)piperazine-1-ethanesulfonic acid), *N*-(2-hydroxyethyl)piperazine-*N*′-(2-ethanesulfonic acid) was added to the medium to maintain the pH at a value of 7.4–7.7.

Chemical treatment for disrupting the cell cytoskeleton. Cells were treated with 5 μM cytochalasin D (Sigma-Aldrich) to depolymerize the actin filaments. This step was performed *in vivo* by adding Cyt-D to the cell medium during the AFM measurements.

3.3 Finite element simulations

The numerical simulations of the indentation were performed using commercial Finite Element Method software (COMSOL Multiphysics, COMSOL AB, Stockholm, Sweden). The indenter was a sphere of radius R = 5 μm, and the material model used for it was a linear elastic material (isotropic and homogeneous, E = 20 GPa). The sample was simulated as a cylinder of 40 μm of radius and 40 μm in depth. The indentation depth was very small (0.2 μm) with respect to the thickness of the sample, in order to avoid boundary effects. The mesh size was graded to be more refined close to the indenter (0.02 μm), and coarser at the sides. The simulations were performed assuming a fric-

tionless contact and cylindrical symmetry. The material model for the sample was a linear visoelastic material. COMSOL solves the full 3-D differential equations of viscoelasticity, although experimentally the AFM measurements only provide 1-D data. The values chosen for the viscoelastic parameters of the sample are similar to those obtained in the experiments (E_{cell} = 4 kPa, η = 300 Pa s). To simulate an adhesion force, we have added a negative force that was active during the retraction cycle of the force curve. The absolute value of this attractive force was chosen to be about 44% of the maximum repulsive force.

4. Results and discussion

4.1 Force–distance curves

An optical microscope directs the positioning of the AFM probe onto the surface of a single mouse embryonic fibroblast (MEF) cell to record a force–distance curve (Fig. 1a). An AFM image of a section of the cell shows some features of the cytoskeleton (Fig. 1b).

Fig. 1c shows the z-piezo displacement, the indentation and the force as a function of time during the acquisition of a force curve above the nucleus of a MEF. The raw data represent the variation of the cantilever deflection Δz with respect to the z-piezo displacement $z(t)$. To obtain the force as a function of the tip–cell distance, the cantilever deflection is multiplied by the force constant k and the z-piezo displacement is converted into indentation values I. The latter is achieved using the following relationship,

$$S(t) = z(t) + \Delta z(t) - z_0 \quad (13)$$

with

$$I(t) = -S(t) \text{ for } S \leq 0 \quad (14)$$

where $z(t)$ is the z-piezo displacement; $S(t)$ is the instantaneous tip–sample distance; and z_0 marks the z-piezo displacement at which the tip establishes mechanical contact with the cell surface (approach).

Fig. 1d shows that the approach and retraction sections of the force curve do not coincide. This observation reveals the existence of dissipative interactions between the tip and the cell. The area enclosed by the approach and retraction sections of the force curve coincides with the energy dissipated on the sample.[46,47,50]

4.2 Elastic modulus, loss modulus, viscosity coefficient and relaxation time

To obtain the mechanical properties E, E_{loss}, η and τ from the force–distance curve, it is required to determine the conserva-

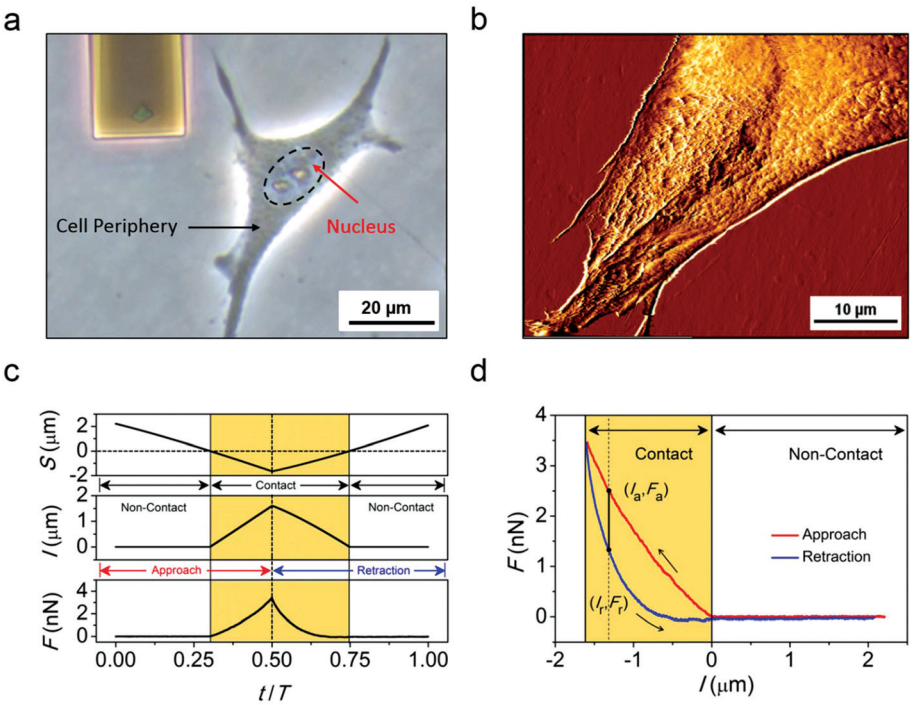

Fig. 1 Force–distance curves in nanomechanical rheology. (a) Optical microscopy image of a rectangular microcantilever in the proximity of a fibroblast cell. The black dashed line indicates the edges of the nucleus. The image has been taken using an inverted optical microscope. The pyramidal tip appears at the end of the cantilever. (b) AFM image of a MEF cell. The image reveals the existence of several elements of the cytoskeleton structure. (c) Tip–sample distance, indentation and force as a function of the ratio between the time elapsed and the period of the modulation (approach and retraction). (d) Force *versus* distance curve on top of a MEF cell. The hysteresis loop indicates the presence of dissipative interactions between the tip and the cell.

tive F_c and dissipative components F_{dis} of the interaction force. For a given indentation I, we combine the values of the force during the approach (F_a) and retraction (F_r) cycles of the force curve to obtain F_c and F_{dis},

$$F_c(I) = \frac{F_a(I) + F_r(I)}{2} \quad (15)$$

$$F_{dis}(I) = \frac{F_a(I) - F_r(I)}{2} \quad (16)$$

If the approach and retraction sections of the force–distance curve overlap, $F_a(I) = F_r(I)$ and $F_{dis} = 0$.

For a conical tip, we obtain

$$F_c(I) = \frac{F_a(I) + F_r(I)}{2} = \frac{8}{3}\frac{\tan(\varphi)}{\pi} EI^2 \quad (17)$$

$$F_{dis}(I) = F_{vis}(I) = \frac{\Delta F}{2} = 8\frac{\tan(\varphi)}{\pi}\eta I\left[\frac{dI_a}{dt} - \frac{dI_r}{dt}\right] \quad (18)$$

We also assume that for a given indentation $I(t)$, $dI_a/dt \approx -dI_r/dt$.

4.3. Viscoelastic contact area

The contact area in AFM experiments is commonly determined by using either Hertz or Sneddon contact mechanics models. However, these models fail to describe the contact area in the presence of viscoelastic processes. To illustrate this effect we have performed finite element simulations (Fig. 2a) in the presence of three different contact mechanics interactions, Hertz, 3D Kelvin–Voigt and a contact mechanics model that includes a 3D Kelvin–Voigt and an adhesion force during the tip retraction. Fig. 2b shows the dependence of the force with respect to the tip motion for the above models. The force is normalized to the maximum value per cycle given by Hertz contact mechanics. The introduction of a linear viscoelastic interaction increases the force during the tip approach with respect to Hertz contact mechanics. The maximum value of the repulsive force (peak force) is reached well before the tip produces the maximum indentation. The viscous force depends on the tip velocity, see eqn (9). The maximum in the force reflects the competition between the elastic and dissipative effects. The elastic force increases with the indentation while the dissipative force depends on both the indentation and its time derivative. The indentation rate decreases upon contact with the cell. At the maximum indentation, the viscous force disappears because the indentation rate is zero. Consequently, all the models give the same value for the force.

Fig. 2c shows the radius a of the contact area of a linear viscoelastic body that interacts with a spherical tip. The contact area is defined as the area of the contact projected on a plane perpendicular to the tip indentation (πa^2). The radius is presented as a function of the time. However, it could be easily transformed into a function of the indentation using eqn (13) and (14). During the approach, the contact is characterized by a contact radius that follows the shape and the numerical values given by Hertz contact mechanics. During the tip retraction, the contact radius of the viscoelastic body decreases more rapidly than that of an elastic material. This effect is somehow reduced by the presence of an adhesion force in the retraction section (red dots). The mechanical response of the body has been simulated with an elastic modulus of 4 kPa and a viscous coefficient of 300 Pa s. These values are similar to those obtained for a MEF cell (see below).

The above comparison shows that during the tips approach and near the maximum indentation, the contact area of the deformation of a linear viscoelastic body is well approximated by the contact area obtained from an elastic contact mechanics model.

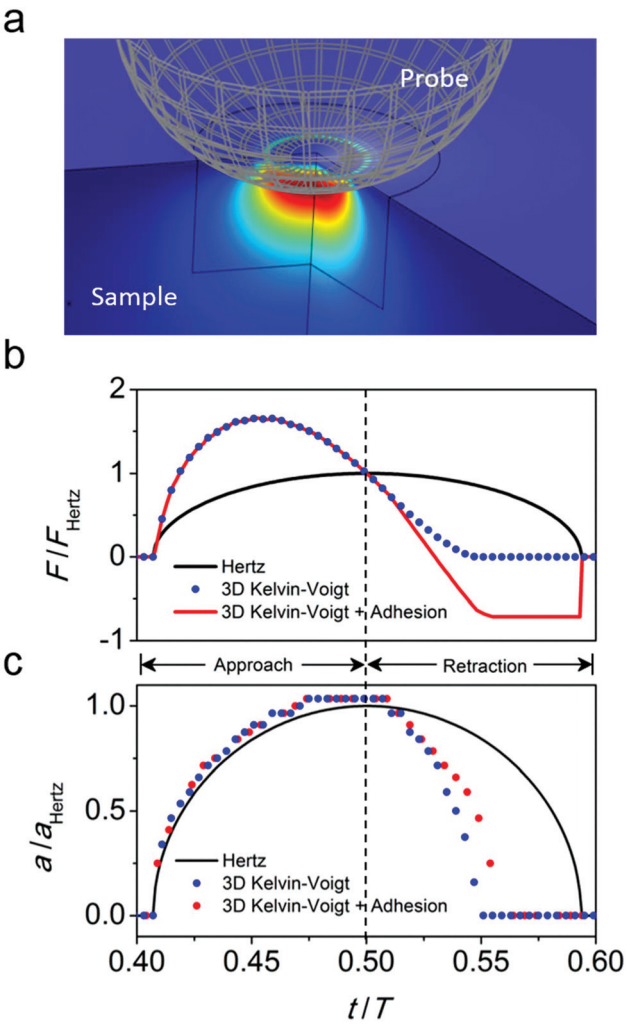

Fig. 2 Finite element simulations of the deformation of a soft sample. (a) Finite element simulation of a force microscope–soft matter interface. The color-code variations on the sample indicate the changes in the stress. (b) Force *versus* time curves obtained from finite element simulations. Three contact mechanics interactions are considered, Hertz, Kelvin–Voigt and Kelvin–Voigt with an adhesion force. The force is normalized with respect the maximum value given by Hertz contact mechanics. (c) Contact area (radius) dependence on the time for the interactions described in (b). All the finite element simulations have been performed with the following parameters: E_{cell} = 4 kPa, η_{com} = 300 Pa s; f_m = 1 Hz, R = 5 μm (colloidal tip); F_{Hertz}(max) = 1.4 nN.

4.4. Nanomechanical rheology of a mice embryonic fibroblast cell

We have applied the above method to determine the nanomechanical response of a single cell subjected to external forces of varying modulation frequencies. Fig. 3 shows the dependence of the elastic modulus, the viscosity coefficient, the loss modulus and the relaxation time as a function of the modulation frequency in the 0.2 to 4 Hz range. In this frequency range, the elastic modulus remains practically constant at 5 kPa, and the viscosity coefficient decreases from 460 Pa s to 60 Pa s. The loss modulus shows two regimes. For modulation frequencies in the 0.2–2 Hz range, E_{loss} increases monotonically from 3 to 3.7 kPa. For higher frequencies, it appears to oscillate around a value of 3.8 kPa. The relaxation time decreases exponentially from 0.28 s at 0.2 Hz to 0.05 s at 4 Hz. Each data point is the average value of 10 force–distance curves.

Two relevant conclusions are derived from the data shown in Fig. 3. First, there is not a general trend in the dependence with respect to the frequency. The above observation implies that to understand and characterize the nanorheology of a single cell it is required to measure several parameters. Second, live cells show significant changes in the mechanical response in a relatively small frequency range.

The data shown in Fig. 3 report the measurements performed on a single cell. We have repeated the measurements on 20 different MEF cells. All the cells reproduced the frequency dependencies described in Fig. 3.

4.5. Time-resolved response of a cell to cytochalasin D

Previous AFM studies have underlined the influence of the actin cytoskeleton structure on the elastic response of cells.[4,54] Those studies measured the changes in the cell stiffness in the presence of different drugs, in particular, cytochalasin D (Cyt-D). This drug inhibits the polymerization of the actin which eventually produces the fragmentation of the actin filaments. We have applied the above nanomechanical rheology method to follow the evolution in the mechanical response of a single MEF cell subjected to the action of Cyt-D.

To simplify the discussion we limit the measurements to a single modulation frequency (1 Hz). Fig. 4a shows some optical microscopy images that illustrate the shape changes of a MEF under the action of Cyt-D (see the ESI:† time evolution of the MEFs affected by the Cyt-D). The cell increases its volume and becomes more rounded in the presence of Cyt-D. The evolution of the elastic modulus, the viscosity coefficient, the loss modulus and the relaxation time as a function of the exposure time to Cyt-D is shown in Fig. 4b–e. The elastic modulus of the cell decreases in the presence of Cyt-D. These results are in agreement with previous studies.[4,53] However, the method allows us to observe three time domains. First, there is a sharp decrease from 6.2 kPa to 3.6 kPa that happens within the first 5 minutes. This decrease is characterized by a slope of -10 Pa s^{-1}. Between 5 and 30 minutes, the elastic modulus changes from 3.6 to 1.6 kPa. The rate is reduced to -1 Pa s^{-1}. After 30 minutes, the elastic

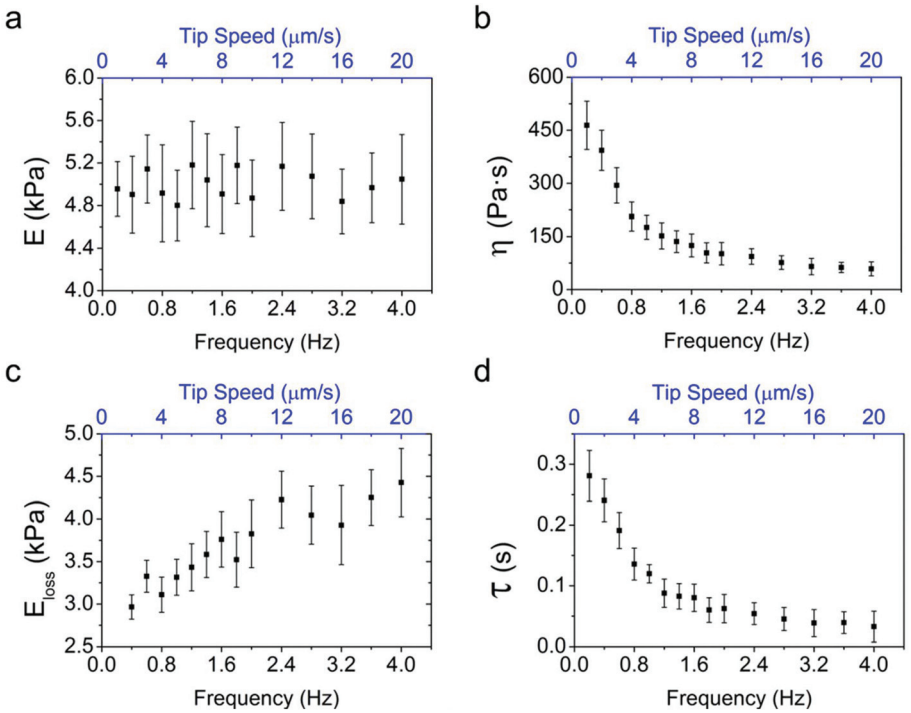

Fig. 3 Frequency dependence of the nanomechanical response of a single MEF cell in culture medium. (a) Elastic modulus. (b) Loss modulus. (c) Viscosity coefficient. (d) Relaxation time. For completeness we also plot the cantilever speed associated with each modulation frequency.

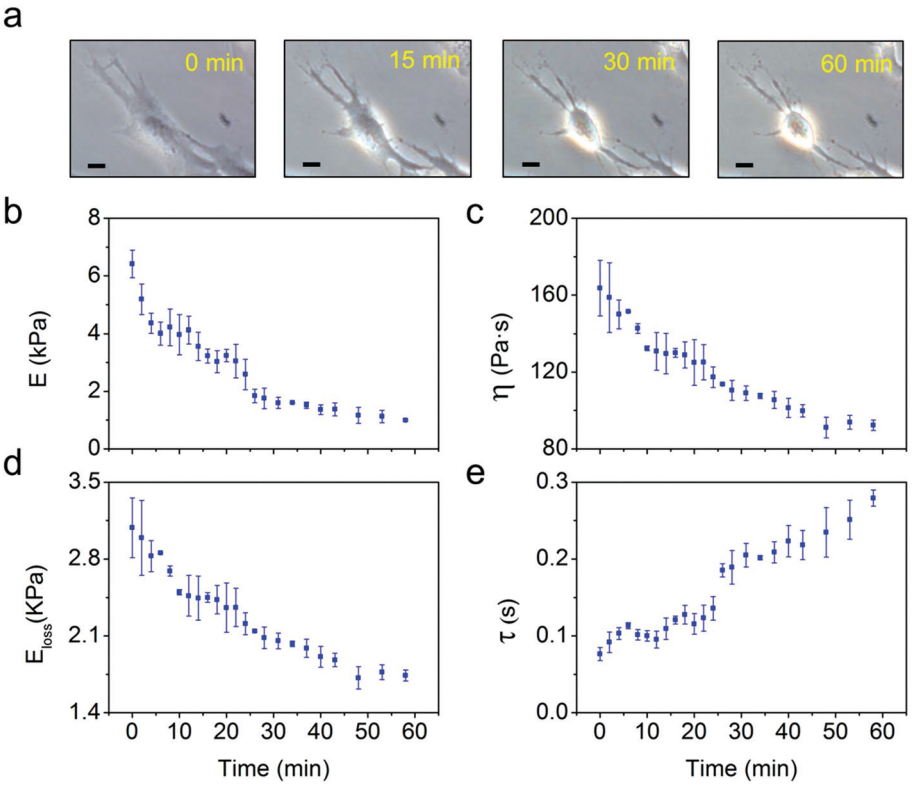

Fig. 4 Time-resolved nanomechanical response of a single cell under the action of a drug. (a) Sequence of images (optical microscopy) of a MEF cell exposed to cytochalasin D. The scale bars correspond with 10 μm. (b) Elastic modulus dependence on the exposure time. (c) Viscosity coefficient. (d) Loss modulus. (e) Relaxation time. The data have been acquired for a modulation frequency of 1 Hz.

modulus decays very slowly towards 1 kPa with a slope close to −0.3 Pa s^{-1}. The above results are in contrast with the trend observed for the viscosity coefficient and the loss modulus. The viscosity coefficient decreases monotonically with time from 165 Pa s to 90 Pa s. The loss modulus decreases from 3.2 Pa to 1.7 kPa. The rate is −0.4 Pa s^{-1}. The relaxation time increases with the exposure time from 0.07 s to 0.28 s. The relaxation time reflects a competition between elastic and dissipative processes within the cell. The treatment with Cyt-D softens the cytoskeleton structure and reduces the viscous flow. However, the softening of the cell happens at a faster rate that the reduction of the viscosity, thus, the increase of τ as the exposure time increases.

The above results are consistent with the behavior described by the poroelastic model.[26,54] In this model, the cytoplasm consists of a porous, elastic solid (cytoskeleton, organelles, ribosomes) filled with an interstitial fluid (cytosol) that moves through the pores in response to pressure gradients. The disruption of the F-actin polymerization weakens the cytoskeleton architecture, and as a consequence the elastic modulus decreases. On the other hand, the fragmentation of the acting filaments is equivalent to the increased average pore size. If the size of the pores is increased it becomes easier to displace the cytosol through the cytoplasm, and then the viscosity decreases.

5. Conclusions

We have developed a nanomechanical rheology method to measure the time and frequency dependencies of the response of a single live cell to an external force. This method provides four parameters, the elastic modulus, the viscosity coefficient, the loss modulus and the relaxation time. These parameters exhibit different frequency dependencies. At low modulation frequencies (0.2–4 Hz), the elastic modulus remains unchanged; the loss modulus increases while the viscosity coefficient and the relaxation time decrease. The above results underline the limited information about the mechanical state of a cell provided by stiffness measurements. We show that the mechanical response of live fibroblast cells has significant changes in the 0.2 to 4 Hz frequency range. The above results imply that to understand and characterize the nanorheology of a single cell it is required to measure several parameters.

The method has been applied to follow the evolution of a fibroblast cell subjected to the depolymerization of its F-actin cytoskeleton with a time resolution of 1 minute. The loss modulus and the viscous coefficient monotonically decrease with the exposure time to the cytochalasin D. The relaxation time increases with the exposure time from 0.07 s to 0.28 s. The elastic modulus has three different time domains. First, there is a sharp decrease from 6.2 kPa to 3.6 kPa that happens within the first 5 minutes. Between 5 and 30 minutes, the

elastic modulus changes from 3.6 to 1.6 kPa. After 30 minutes, the elastic modulus decays very slowly towards 1 kPa with a slope close to -0.3 Pa s^{-1}. The proposed method is general. It can be applied to study different types of cells and different types of cell–drug interactions.

The above behavior is compatible with a cell mechanical response described by the poroelastic model. The fragmentation of the actin filaments reduces the elastic modulus. At the same time, the depolymerization of the actin filaments leads to an increase of the average size of the cytoskeleton pores, which increases the cytosol flow. This process is equivalent to a reduction of the viscosity coefficient. The increase of the relaxation time implies that the weakening of the cytoskeleton structure as measured by the elastic modulus is a factor that dominates over the reduction of the viscosity.

Acknowledgements

We thank financial support from the European Research Council ERC – AdG – 340177 (3DNanoMech) and the Ministerio de Economía y Competitividad (CSD2010-00024), MAT2016-76507-R.

Notes and references

1 D. J. Müller and Y. F. Dufrene, *Trends Cell Biol.*, 2011, **21**(8), 461–469.
2 M. P. Stewart, J. Helenius, Y. Toyoda, *et al.*, *Nature*, 2011, **469**(7329), 226–230.
3 K. Haase and A. E. Pelling, *J. R. Soc., Interface*, 2015, **12**, 20140970.
4 C. Rotsch and M. Radmacher, *Biophys. J.*, 2000, **78**, 520–553.
5 M. Prass, K. Jacobson, A. Mogilner, *et al.*, *J. Cell Biol.*, 2006, **174**(6), 767–772.
6 C. Roduit, S. Sekatski, G. Dietler, S. Catsicas, F. Lafont and S. Kasas, *Biophys. J.*, 2009, **97**, 674–677.
7 N. Gavara and R. S. Chadwick, *Nat. Nanotechnol.*, 2012, **7**, 733–736.
8 A. Raman, S. Trigueros, A. Cartagena, A. P. Z. Stevenson, M. Susilo, E. Nauman and S. A. Contera, *Nat. Nanotechnol.*, 2011, **6**, 809–814.
9 R. Vargas-Pinto, H. Gong, A. Vahabikashi and M. Jonhson, *Biophys. J.*, 2013, **105**, 300–309.
10 J. R. Staunton, B. L. Doss, S. Lindsay and R. Ross, *Sci. Rep.*, 2016, **6**, 19686.
11 A. Rigato, F. Rico, F. Eghiaian, M. Piel and S. Scheuring, *ACS Nano*, 2015, **9**(6), 5846–5856.
12 M. Lekka, P. Laidler, D. Gil, J. Lekki, Z. Stachura and A. Z. Hrynkiewicz, *Eur. Biophys. J.*, 1999, **28**(4), 312–316.
13 M. Lekka, K. Pogoda, J. Gostek, O. Klymenko, S. Prauzner-Bechcicki, J. Wiltowska-Zuber, J. Jaczewska, J. Lekki and Z. Stachura, *Micron*, 2012, **43**(12), 1259–1266.
14 S. E. Cross, Y.-S. Jin, J. Rao and J. K. Gimzewski, *Nat. Nanotechnol.*, 2007, **2**, 780–783.
15 S. Iyer, R. M. Gaikwad, V. Subba-Rao, *et al.*, *Nat. Nanotechnol.*, 2009, **4**(6), 389–393.
16 M. Plodinec, *et al.*, *Nat. Nanotechnol.*, 2012, **7**, 757–6514.
17 J. R. Ramos, J. Pabijan, R. Garcia and M. Lekka, *Beilstein J. Nanotechnol.*, 2014, **5**, 447–457.
18 H. Oberleithner, C. Riethmüller, H. Schillers, G. A. MacGregor, H. E. de Wardener and M. Hausberg, *Proc. Natl. Acad. Sci. U. S. A.*, 2007, **104**, 16281–16286.
19 A. Reich, M. Meurer, B. Eckes, J. Friedrichs and D. J. Muller, *J. Cell. Mol. Med.*, 2009, **13**, 1644–1652.
20 A. Fuhrmann, J. R. Staunton, V. Nandakumar, *et al.*, *Phys. Biol.*, 2011, **8**(1), 015007.
21 D. Xia, S. Zhang, J. Ø. Hjordal, Q. Li, K. Thomsen, J. Chevallier, F. Besenbacher and M. Dong, *ACS Nano*, 2014, **10**(7), 6873–6882.
22 S. Zhang, H. Aslan, F. Besenbacher and M. Dong, *Chem. Soc. Rev.*, 2014, **43**, 7412.
23 J. G. Goetz, S. Minguet, I. Navarro-Lérida, J. J. Lazcano, R. Samaniego, E. Calvo, M. Tello, T. Osteso-Ibáñez, T. Pellinen, A. Echarri, *et al.*, *Cell*, 2011, **146**, 148–163.
24 S. Zhang, F. L. Bach-Gansmo, D. Xia, F. Besenbacher, H. Birkedal and M. Dong, *Nano Res.*, 2015, **8**(10), 3250–3260.
25 L. Blanchoin, R. Boujemaa-Paterski, C. Sykes and J. Plastino, *Physiol. Rev.*, 2014, **94**, 235–263.
26 E. Moendarbary, G. T. Charras, *et al.*, *Nat. Mater.*, 2013, **12**, 253–261.
27 P. Bursac, G. Lenormand, B. Fabry, M. Oliver, D. A. Weitz, V. Viasnoff, J. P. Butler and J. J. Fredberg, *Nat. Mater.*, 2005, **4**(7), 557–561.
28 R. E. Mahaffy, C. K. Shih, F. C. MacKintosh and J. Käs, *Phys. Rev. Lett.*, 2000, **85**, 880–883.
29 J. Rother, H. Nöding, I. Mey and A. Janshoff, *Open Biol.*, 2014, **4**, 140046.
30 A. Calzado-Martin, M. Encinar, J. Tamayo, M. Calleja and A. San Paulo, *ACS Nano*, 2016, **10**, 3365–3374.
31 C. A. Amo and R. Garcia, *ACS Nano*, 2016, **10**, 7117–7124.
32 Y. F. Dufrene, D. Martinez-Martin, I. Medalsy, D. Alsteens and D. J. Müller, *Nat. Methods*, 2013, **10**, 847–854.
33 J. Alcaraz, L. Buscemi, M. Grabulosa, X. Trepat, B. Fabry, R. Farre and D. Navajas, *Biophys. J.*, 2003, **84**, 2071–2079.
34 V. Vadillo-Rodriguez, T. J. Beveridge and J. R. J. Dutcher, *J. Bacteriol.*, 2008, **190**(12), 4225–4232.
35 S. Moreno-Flores, R. Benitez, M. dM. Vivanco, *et al.*, *Nanotechnology*, 2010, **21**(44), 445101.
36 A. Cartagena and A. Raman, *Biophys. J.*, 2014, **106**, 1033–1043.
37 F. M. Hecht, J. Rheinlaender, N. Schierbaum, W. H. Goldmann, B. Fabry and T. E. Schäffer, *Soft Matter*, 2015, **11**, 4584.
38 E. Fischer-Friedrich, Y. Toyoda, C. J. Cattin, D. J. Müller, A. A. Hyman and F. Julicher, *Biophys. J.*, 2016, **111**, 589–600.

39 A. X. Cartagena-Rivera, W. H. Wang, R. L. Geahlen and A. Raman, *Sci. Rep.*, 2015, **5**, 11692.
40 E. A. Lopez-Guerra and S. D. Solares, *Beilstein J. Nanotechnol.*, 2014, **5**, 2149–2163.
41 M. Chyasnavichyus, S. L. Young and V. V. Tsukruk, *J. Appl. Phys.*, 2015, **54**, 8S2.
42 S. R. Cohen and E. Kalfon-Cohen, *Beilstein J. Nanotechnol.*, 2013, **4**, 815–833.
43 S. D. Solares, *Beilstein J. Nanotechnol.*, 2015, **6**, 2233–2241.
44 R. Proksch and D. G. Yablon, *J. Appl. Phys.*, 2016, **119**, 134901.
45 C. Rianna and M. Radmacher, *Eur. Biophys. J.*, 2016, **46**(4), 309–324.
46 J. Tamayo and R. Garcia, *Appl. Phys. Lett.*, 1998, **73**, 2926.
47 R. Garcia, R. Magerle and R. Perez, *Nat. Mater.*, 2007, **6**, 405–411.
48 S. Nawaz, P. Sanchez, K. Bodensiek, S. Li, M. Simons and I. A. T. Schaap, *PLoS One*, 2012, **7**(9), e45297.
49 L. M. Rebelo, J. S. de Sousa, J. M. Filho and R. Radmacher, *Nanotechnology*, 2013, **24**, 055102.
50 R. Garcia, C. J. Gomez, N. F. Martinez, S. Patil, C. Dietz and R. Magerle, *Phys. Rev. Lett.*, 2006, **97**, 016103.
51 K. L. Johnson, *Contact Mechanics*, Cambridge University Press, Cambridge, 1985.
52 N. W. Tschoegl, *The phenomenological theory of linear viscoelastic behavior: an introduction*, Springer-Verlag, Berlin, Heidelberg, 1989.
53 E. H. Lee and J. R. M. Radok, *J. Appl. Mech.*, 1960, **27**(3), 438–444.
54 A. R. Harris and G. T. Charras, *Nanotechnology*, 2011, **22**, 345102.
55 C. P. Green and J. E. Sader, *J. Appl. Phys.*, 2005, **98**, 114913.
56 S. Basak, A. Raman and S. V. Garimella, *J. Appl. Phys.*, 2006, **99**, 14906.